Biomaterials 32 (2011) 7226–7233

Contents lists available at ScienceDirect

Biomaterials

journal homepage: www.elsevier.com/locate/biomaterials

Single-phased luminescent mesoporous nanoparticles for simultaneous cell imaging and anticancer drug delivery

Weihua Di [a,b,c,*], Xinguang Ren [d], Haifeng Zhao [d], Naoto Shirahata [c,e], Yoshio Sakka [b,c,**], Weiping Qin [a,***]

[a] State Key Laboratory on Integrated Optoelectronics, College of Electronic Science and Engineering, Jilin University, Changchun 130012, PR China
[b] World Premier International Research (WPI) Center Initiative on Materials Nanoarchitronics (MANA), National Institute for Materials Science (NIMS), 1-2-1 Sengen, Tsukuba, Ibaraki 305-0047, Japan
[c] Advanced Ceramics Group, Advanced Materials Processing Unit, NIMS, 1-2-1 Sengen, Tsukuba, Ibaraki 305-0047, Japan
[d] Key Laboratory of Excited-state Processes, Changchun Institute of Optics, Fine Mechanics and Physics, Chinese Academy of Sciences, 3888 Eastern South Lake Road, Changchun 130033, PR China
[e] PRESTO, Japan Science and Technology Agency (JST) 4-1-8 Honcho Kawaguchi, Saitama 332-0012, Japan

ARTICLE INFO

Article history:
Received 25 May 2011
Accepted 9 June 2011
Available online 13 July 2011

Keywords:
Lanthanide oxides
Mesopore
Luminescence
Cell imaging
Drug delivery
Cytotoxicity

ABSTRACT

Multifunctional materials for biological use have mostly been designed with composite or hybrid nanostructures in which two or more components are incorporated. The present work reports on a multifunctional biomaterial based on single-phased luminescent mesoporous lanthanide oxide nanoparticles that combine simultaneous drug delivery and cell imaging. A simple strategy based on solid-state-chemistry thermal decomposition process was employed to fabricate the spherical mesoporous Gd_2O_3:Eu nanoparticles with homogeneous size distribution. The porous nanoparticles developed by this strategy possess well-defined mesopores, large pore size and volume, and high specific surface area. The mesoporous features of nanoparticles impart the material with capabilities of loading and releasing the drug with a relatively high loading efficiency and a sustained release behavior of drugs. The DOX-loaded porous Gd_2O_3 nanoparticles are able to kill the cancer cells efficiently upon incubation with the human cervical carcinoma (HeLa) cells, indicating the potential for treatment of cancer cells. Meanwhile, the intrinsic luminescence of Gd_2O_3:Eu nanoparticles gives the function of optical imaging. Therefore, the drug release activity and effect of drugs on the cells can be effectively monitored via luminescence of nanoparticles themselves, realizing multifunctionality of simultaneous cell imaging and anticancer drug delivery in a single-phased nanoparticle.

1. Introduction

Many drugs, especially cancer-therapy drugs, have severe side effect that is caused by the nonspecific uptake of anticancer drugs by healthy tissues/organs such as kidney, liver, bone marrow and heart. Encapsulation of such drugs in carriers could reduce these side effects significantly, because a carrier can protect organs from a toxic drug and prevent the decomposition/denaturing of the drugs prior to reaching the targeted cells [1,2]. Moreover, encapsulation enables drugs to be released in a controlled way [1–3].

Mesoporous materials have been shown as a potentially useful drug carrier because of their unique characteristics such as high surface area, tunable pore size and volume, and well-defined surface properties for modifications [3–5]. To achieve multifunctional purpose of biological use of porous materials, extensive efforts have been devoted to designing a composite or hybrid nanostructure in which two or more components are incorporated to give the final material multifunctional capabilities. Therefore, the fabrication of the heterostructured mesoporous particles has attracted considerable attention in recent years, since they can combine the drug delivery with other biological functions, such as fluorescence imaging and magnetic resonance (MR) imaging or both into a composite/hybrid nanostructure, thus simultaneously fulfilling multifunctionalities [2,6–12]. A thin layer of mesoporous silica is coated onto the $NaYF_4$ up-conversion nanocrystals to form core-shell $NaYF_4$@silica nanoparticles for synergistic imaging and

* Corresponding author. State Key Laboratory on Integrated Optoelectronics, College of Electronic Science and Engineering, Jilin University, Changchun 130012, PR China.
** Corresponding author. World Premier International Research (WPI) Center Initiative on Materials Nanoarchitronics (MANA), National Institute for Materials Science (NIMS), 1-2-1 Sengen, Tsukuba, Ibaraki 305-0047, Japan
*** Corresponding author.
E-mail addresses: weihdi@yahoo.com.cn (W. Di), SAKKA.Yoshio@nims.go.jp (Y. Sakka), wpqin@jlu.edu.cn (W. Qin).

0142-9612/$ – see front matter © 2011 Elsevier Ltd. All rights reserved.
doi:10.1016/j.biomaterials.2011.06.019

photodynamic therapy (PDT) [6]. The mesoporous silica particles were functionalized by the deposition of luminescent YVO_4:Eu layer for drug carriers. Simultaneously, the behaviors of drug loading and release of mesoporous silica can be efficiently monitored via luminescence of YVO_4:Eu as a function of drug loading and release amount [7]. Superparamagnetic iron oxide nanocrystals were encapsulated inside mesostructured silica spheres that were labeled with fluorescent dye molecules, to endow the resulting material with multiple capabilities of dual-imaging (optical and MR) and drug storage and release [8]. Clearly, such multicomponent composite nanostructures can provide a platform for multifunctional biological uses.

However, the construction of a multicomponent composite nanostructure involves multistep synthetic procedures, and sometimes requires stringent synthetic conditions [12,13]. In some cases, some toxic surfactants or solvents are needed to add into the reaction system, which renders the final material with significant toxicity [14]. Furthermore, the formation of a composite structure commonly results in the performance degradation of individual component and inhomogeneity of the morphology and properties of the resulting material, remarkably limiting its final applications [13].

Herein, in this work, we have developed single-phased luminescent spherical mesostructured Gd_2O_3:Eu nanoparticles via a simple solid-state-based thermal decomposition process of lanthanide complex sources. The intrinsic strong luminescence and mesoporous nature impart the nanoparticles with the capabilities of simultaneous optical imaging and anticancer drug storage and delivery in a single-phased material.

2. Experimental

2.1. Preparation of $Gd(OH)CO_3$ H_2O:Eu.

The monodisperse $Gd(OH)CO_3 \cdot H_2O$ colloidal nanoparticles were prepared via a urea-based homogeneous precipitation process. A total of 5 mL of $Gd(NO_3)_3$ (1 M) and 10 g of urea $[CO(NH_2)_2]$ were dissolved in deionized water. The total volume of the solution was about 250 mL. The above solution was first homogenized under magnetic stirring at room temperature for 2 h. The resultant solution was then reacted at 85 °C for 2.5 h in an oil bath. The obtained suspension was separated by centrifugation and collected after washing with deionized water and ethanol several times. Eu^{3+}-doped samples were obtained under the same conditions by replacing a fraction of $Gd(NO_3)_3$ by $Eu(NO_3)_3$.

2.2. Preparation of mesoporous Gd_2O_3:Eu.

Mesoporous gadolinium oxides (Gd_2O_3:Eu) were obtained by calcinating the as-prepared $Gd(OH)CO_3 \cdot H_2O$:Eu at 750 °C for 2 h with a heating rate of 2 °C min^{-1}.

2.3. Characterizations.

The X-ray powder diffraction (XRD) data were collected on an X'Pert MPD Philips diffractometer (CuKα X-radiation at 40 kV and 50 mA) in the 2θ range from 15° to 70° with a scanning step of 0.02°. The transmission electron microscopy (TEM) observations were carried our using a JEOL 2200FS microscope. Samples for TEM investigations were prepared by first dispersing the particles in ethanol under assistance of ultrasonification and then dropping 1 drop of the suspension on a copper TEM grid coated with a holey carbon film. Fourier transform infrared (FT-IR) spectra (Mattson 5000) of the samples were measured in the range of 4000-500 cm^{-1} in transmission mode. The pellets were prepared by adding 0.8 mg of the sample powder to 80 mg of KBr. The powders were mixed homogeneously and compressed at a pressure of 10 kPa to form transparent pellets. Thermogravimetric analysis (TGA) of the as-prepared precursor was performed using a thermoanalyzer (Thermo Plus TG 8120, Rigaku). The data were recorded at a scan rate of 5 °C min^{-1} from room temperature to 800 °C in air. The N_2 adsorption-desorption isotherms were recorded at 77 K on a Micromeritics ASAP 2010. The samples were degassed at 523 K and 10^{-6} Torrr for 10 h prior to measurement. UV–Vis absorbance measurements were carried out by a single-beam spectrophotometer (U-2900, Hitachi) equipped with a 75-W pulsed xenon lamp with a scan rate of 240 nm min^{-1}. The fluorescence spectra were recorded on a fluorescence spectrophotometer (F-7000, Hitachi) at room temperature. The slit widths of the excitation and emission were both 1.0 nm. The luminescence quantum yield was taken on Fluorescence SENS-9000 PL calibrated spectrometer equipped with an integrated sphere. Three measurements were made for each sample and the average value is reported. The method is accurate to within 5%.

2.4. Cell culture

HeLa cell lines were maintained in Dulbecco's modified Eagle's medium (DMEM) containing 10% fetal bovine serum (FBS), penicillin (100 units mL^{-1}), and streptomycin (100 mg mL^{-1}). Cells were cultured with the complete medium in 5% CO_2 at 37 °C. For all experiments, cells were harvested from subconfluent cultures by the use of trypsin and were resuspended in fresh complete medium before plating.

2.5. Cellular uptake and observation

In a typical procedure, 7.5×10^4 cells were plated in a 35-mm petri dish for 4 h to allow the cells to attach. After the cells were washed twice with phosphate-buffered saline (PBS), Gd_2O_3:Eu nanoparticles were added to the petri dishes. After incubation for 4–24 h, the cells were washed several times with PBS to remove the remaining particles and dead cells, and then observed under a two-photon laser scanning confocal microscope (TCS SP5, Leica), operating around a 380 nm excitation wavelength using a tunable Chameleon XR laser system.

2.6. Cytotoxicity assay

In vitro cytotoxicity were assessed using 3-(4,5-dimethylthiazol-2-yl)-2,5 diphenyltetrazolium bromide (MTT) reduction assays. In a typical procedure, 2000 cells were plated in 96-well plates for 24 h to allow the cells to attach, and then incubated with Gd_2O_3:Eu particles in 5% CO_2 at 37 °C. At the end of the incubation time, the medium containing Gd_2O_3:Eu particles was removed, and MTT solution (200 mL, diluted in a culture medium to a final concentration of 1 mg mL^{-1}) was added, then the mixture was incubated for another 4 h. The medium was then replaced with dimethyl sulfoxide (200 mL), and the absorbance was monitored with a microplate reader at a wavelength of 570 nm. The cytotoxicity was expressed as the percentage of cell viability compared to that of untreated control cells.

2.7. DOX loading

50 mg of mesoporous Gd_2O_3:Eu nanoparticles were mixed with 5 mL of DOX solution in PBS (0.4 mg/mL). After stirring for 24 h under dark conditions, the DOX-loaded particles were centrifuged and washed with PBS (5 mL). The particles were redispersed in PBS (1 mL) for subsequent tests of *in vitro* DOX release and cytotoxcity

against HeLa cells. To evaluate the DOX-loading efficiency, the UV–vis absorption spectroscopy was used to measure the absorption of the supernatant and washed solutions at a wavelength of 233 nm.

2.8. DOX release

The above-prepared DOX-loaded Gd_2O_3:Eu particles (15 mg) were immersed in PBS (5 mL, pH 7.4) at 37 °C and shaken at 100 rpm. At certain time intervals, aliquots of PBS (5 mL) were taken out by centrifugation to test the concentration of released DOX and fresh PBS (5 mL) was added to the tube containing the DOX-loaded Gd_2O_3 particles. *In vitro* cytotoxicity of DOX-loaded Gd_2O_3 against HeLa cells, HeLa cells were seeded in a 96-well plate at a density of 2000 cells per well and cultured in 5% CO_2 at 37 °C for 24 h. Then, free DOX and DOX-loaded Gd_2O_3 particles were added to the medium, and the cells were incubated in 5% CO_2 at 37 °C for 24–72 h. Cell viability was determined by MTT assay.

3. Results and discussion

3.1. $Gd(OH)CO_3 \cdot H_2O$:Eu as precursor

The precursor to generate luminescent porous gadolinium oxides, Eu-doped gadolinium hydroxylcarbonate hydrate ($Gd(OH)CO_3 \cdot H_2O$:Eu), was prepared via a urea-based homogeneous precipitation method (Experimental section), in which urea serves as a precipitation agent of metal cations due to self decomposition into the OH^- and CO_3^{2-} at elevated temperatures (>83 °C). The urea-based precipitation is a simple and general route for the preparation of lanthanide hydroxylcarbonate that was first developed by Matijevic and his coworkers [15]. The elemental analysis (Table S1, Supplementary Information (SI)), fourier transform infrared spectroscopy (FTIR, Figure S1, SI) and thermogravimetric analysis (Fig. 2, see below) confirmed that the chemical composition of as-prepared precursor is $Gd(OH)CO_3 \cdot H_2O$:Eu. X-ray powder diffraction (XRD) measurement revealed that the as-prepared precursor material is amorphous (Figure S2, SI). These results are consistent with the pioneering work of Matijevic et al. [15] and the recent work by Lechevallier's group [16].

Transmission electron microscopy (TEM) observations (Fig. 1(a) and (b)) revealed that the as-prepared $Gd(OH)CO_3 \cdot H_2O$ particles appear spherical and nearly monodispersed. The size distribution plot (Fig. 1c) based on the analysis of 100 particles from TEM observations indicates that the spherical particle size ranges from 130 to 170 nm with an average diameter of 150 nm and a standard deviation of ±10.6%. The spherical particles with homogeneous monodispersed distribution are preferred for biological uses as it facilitates uniform surface conjugation of cell targeting ligands (e.g., antibodies) and imaging probes [9].

The thermogravimetric analysis (TGA) curve (Fig. 2) of the precursor $Gd(OH)CO_3 \cdot H_2O$:Eu attracted our attention. The weight loss of $Gd(OH)CO_3 \cdot H_2O$ undergoes a three-step process. The first one (25–170 °C) is due to the desorption of water molecules adsorbed at the particles surface due to the storage in air. The second weight loss (170–550 °C) is related to the removal of water molecules due to the dehydration of hydrated compounds and the self-condensation of hydroxyl groups (O-H). This is confirmed by FTIR spectrum of the sample calcinated at 550 °C (Figure S1(b), SI), where the characteristic absorptions of hydration water and hydroxyl groups almost disappear, compared to that of the as-prepared $Gd(OH)CO_3 \cdot H_2O$ (Figure S1(a), SI). The third one (550–750 °C) originates from the release of CO_2 molecules that is also confirmed by FTIR spectrum of the sample calcinated at 750 °C (Figure. S1(c), SI), in which we observed the disappearance of the characteristic vibrations of CO_3^{2-}.

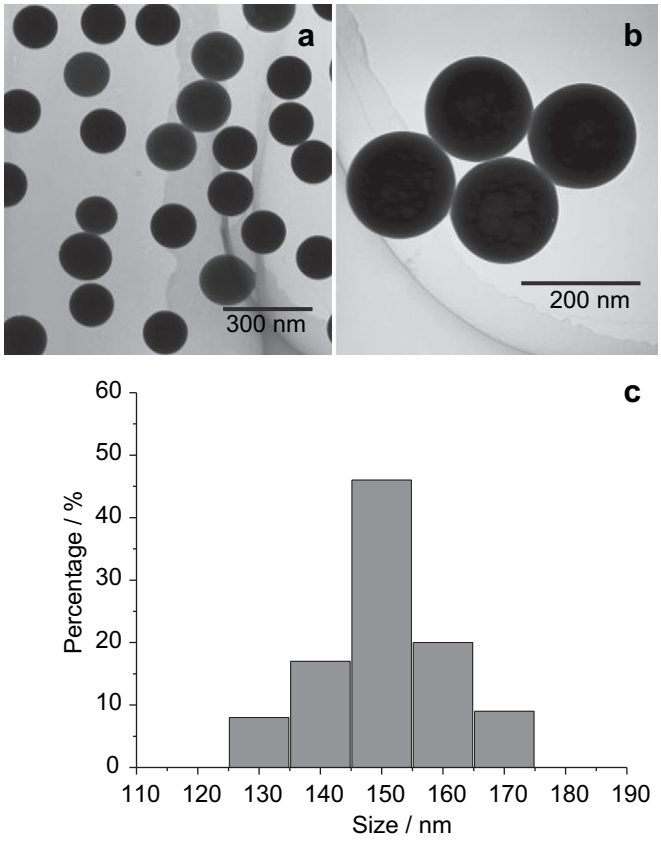

Fig. 1. TEM images of monodispersed and spherical $Gd(OH)CO_3 \cdot H_2O$:Eu particles (a and b) and the size distribution plot based on the analysis of 100 particles from TEM observations (c).

3.2. Mesoporous Gd_2O_3:Eu

What are the composition, structure, morphology, and properties of the product obtained after calcination at 750 °C? Such curiosity inspired our interest to analyze the calcinated sample. XRD characterization reveals that, upon thermal treatment with

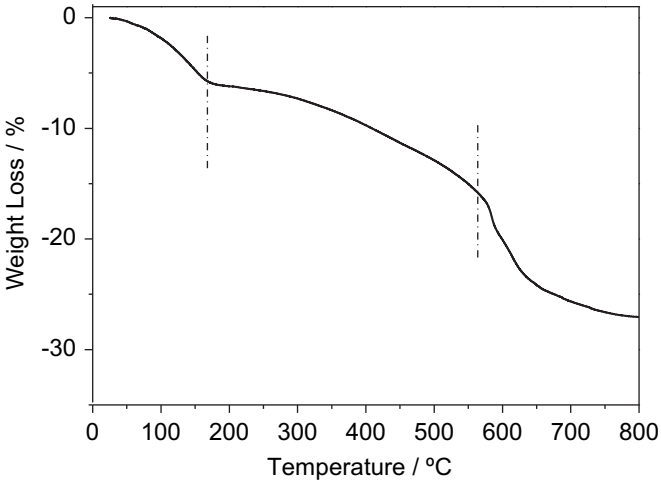

Fig. 2. Thermogravimetric analysis curve of the precursor $Gd(OH)CO_3 \cdot H_2O$:Eu in air.

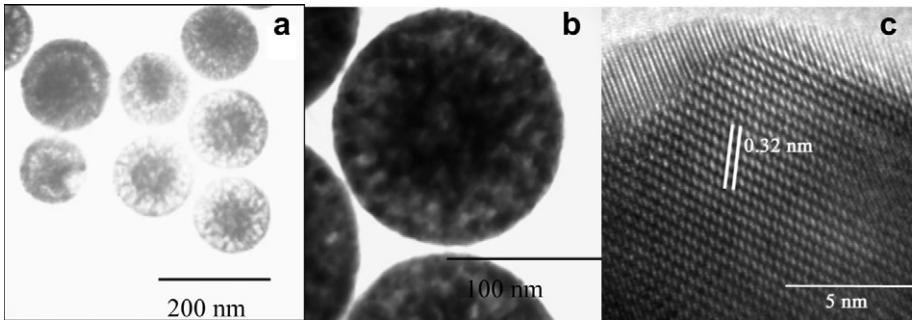

Fig. 3. TEM (a and b) and high resolution TEM (c) images of mesoporous Gd_2O_3:Eu obtained through calcination of as-prepared precursor.

the as-prepared $Gd(OH)CO_3 \cdot H_2O$:Eu up to 750 °C, the amorphous $Gd(OH)CO_3 \cdot H_2O$:Eu is converted and crystallized into gadolinium oxides (Gd_2O_3:Eu) (Figure S2, SI). Combined with the above FTIR and TGA results, the decomposition of the as-prepared $Gd(OH)CO_3 \cdot H_2O$ upon calcination was depicted as follows:

$$2Gd(OH)(CO_3) \cdot H_2O \xrightarrow[-3H_2O]{170^\circ C < T < 550^\circ C} Gd_2O(CO_3)_2 \xrightarrow[-2CO_2]{550^\circ C < T < 750^\circ C} Gd_2O_3 \quad (1)$$

The size and morphology of the sample calcinated at 750 °C were characterized by TEM. The calcinated sample still maintains original size, spherical and monodispersed morphology (Fig. 3) in spite of a high total weight loss up to 30%. This implies there will be large amount of porosity left within the particles. As observed from a representative TEM image, a spherical particle contains tens of small sized nanoparticles (~15 nm, dark regions) that are separated by tens of pores (light regions). These pores were randomly arranged but distributed homogenously throughout the whole particle, and they are large enough (10–15 nm) and uniform with a narrow size distribution. Surprisingly, the framework of the as-prepared precursor particles did not collapse while the mesopore structures were created as a result of the gases burning out during calcination. As a matter of fact, the key to maintain the original particle morphology and create the mesopore structures within the particle is to control the decomposition process at a low heating rate. The rapid heating-up can lead to vigorous gas burst-out, which might destroy the regular morphology of the as-prepared particles and cause the remarkable shrinkages [17]. In our experiment, the heating rate is controlled to be low enough (2 °C min^{-1}) to allow a relatively slow release of gases, which efficiently prevents the remarkable shrinkage of materials and thus leads to the formation of uniform pores surrounding those separated small sized nanoparticles within the original particles. Simultaneously, those small sized nanoparticles separated by the pores are converted and crystallized into gadolinium oxides from the amorphous $Gd(OH)CO_3 \cdot H_2O$:Eu upon thermal treatment. A high resolution TEM image (Fig. 3c) revealed that they are perfectly crystallized without visible defects and dislocations. The calculated interplanar distance is

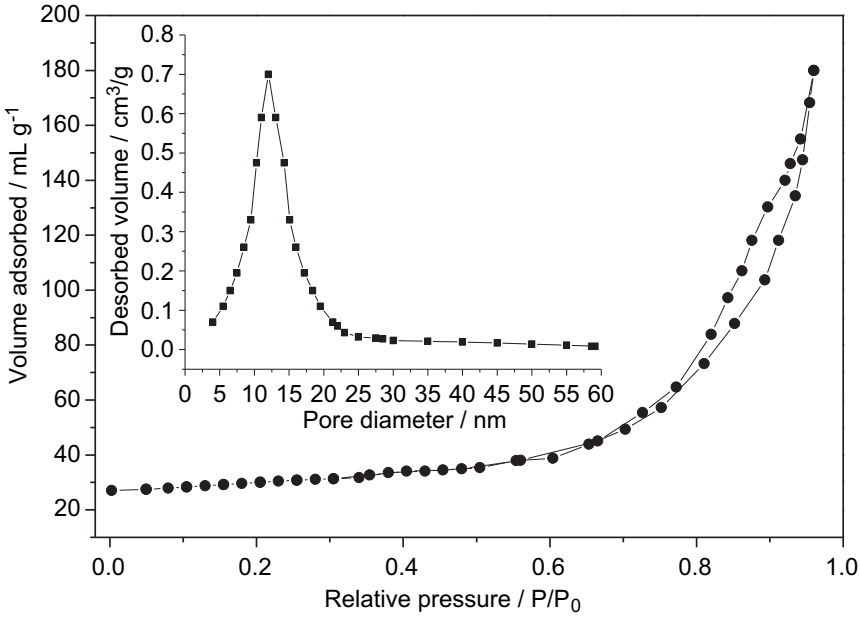

Fig. 4. Nitrogen adsorption-desorption isotherm of mesoporous Gd_2O_3. The inset shows the corresponding pore size distribution curve.

about 0.32 nm, corresponding to the separation of (222) crystal plane of cubic phase Gd_2O_3 that finely matches the XRD result. Therefore, The thermal decomposition of the precursor Gd(OH)$CO_3 \cdot H_2O$:Eu at a temperature up to 750 °C yields uniform, mesoporous and crystalline Gd_2O_3:Eu particles.

Nitrogen adsorption-desorption isotherm (Fig. 4) provides further evidence for the formation of mesoporous Gd_2O_3:Eu derived from thermal decomposition of the precursor Gd(OH)$CO_3 \cdot H_2O$:Eu. The isotherm can be classified as a type IV, which is the characteristic of mesoporous structure. The specific surface area (S_{BET}) calculated with the brunauer-Emmett-Teller (BET) method was increased from 10 m^2/g for Gd(OH)$CO_3 \cdot H_2O$:Eu to 118 m^2/g for the mesoporous Gd_2O_3:Eu. The average pore diameter calculated from the nitrogen adsorption isotherm by the Barrett-Joyner-Halenda (BJH) method was 12.6 nm and the pore size distribution is narrow (inset of Fig. 4). The pore volume for mesoporous Gd_2O_3:Eu is approximately 0.42 $cm^3\ g^{-1}$. The BET measurement of Gd(OH)$CO_3 \cdot H_2O$:Eu shows that no hysteresis-loop of nitrogen adsorption–desorption isotherm was observed (Figure S3, SI), implying that no mesopores exist in the as-prepared precursor, as also observed by TEM (Fig. 1). The difference observed from both samples before and after calcination further confirms that the mesopores within a spherical Gd_2O_3:Eu particle originate from the gases burning out during the thermal decomposition of Gd(OH)$CO_3 \cdot H_2O$:Eu. It is demonstrated that this simple strategy provides a template-free approach for the preparation of nanoporous lanthanide oxides with well-defined mesopores, large pore size and volume, and high specific surface area.

3.3. Luminescence of mesoporous Gd_2O_3:Eu

Lanthanide oxides have been shown to be a useful host lattice for lanthanide ions to produce phosphors emitting a variety of colors (e.g. Gd_2O_3:Eu/Tb, Y_2O_3:Yb,Er) [18–20]. The luminescence of mesoporous Gd_2O_3 doped with Eu^{3+} (5 mol%) was investigated. Fig. 5 shows the room temperature photoluminescence excitation and emission spectra of mesoporous Gd_2O_3:Eu. In the excitation spectrum, a broad band with a maximum at 254 nm originates from the excitation of the oxygen-to-europium charge transfer band (CTB). The observation of the $Gd^{3+}\ ^8S_{7/2} \rightarrow\ ^6I_J$ transition located at 275 nm suggests the existence of Gd^{3+}-to-Eu^{3+} energy transfer [21]. The weak peaks in the longer wavelength region (280–420 nm) are ascribed to the direct f–f transitions within the Eu^{3+} $4f^6$ electron configuration. Upon excitation into a maximum of CTB, the mesoporous Gd_2O_3:Eu emits strong red light that covers the spectrum ranging from 580 to 720 nm due to the $Eu^{3+}\ ^5D_0 \rightarrow\ ^7F_j$ (j = 0,1,2,3,4) transitions. The photoluminescence features were further quantified through the estimation of the absolute emission quantum yield that is measured on a calibrated spectrometer equipped with an integrated sphere. The quantum yield of 0.78 was acquired upon excitation at 254 nm. Such high quantum yield observed for the mesoporous Gd_2O_3:Eu was attributed to the conversion of amorphous Gd(OH)$CO_3 \cdot H_2O$ to highly crystalline Gd_2O_3 and the removal of luminescence quenchers such as H_2O and hydroxyl groups [22]. Strong luminescence and mesoporous nature of our present Gd_2O_3:Eu may be particularly useful for the biological use as fluorescence labels and drug delivery vehicles.

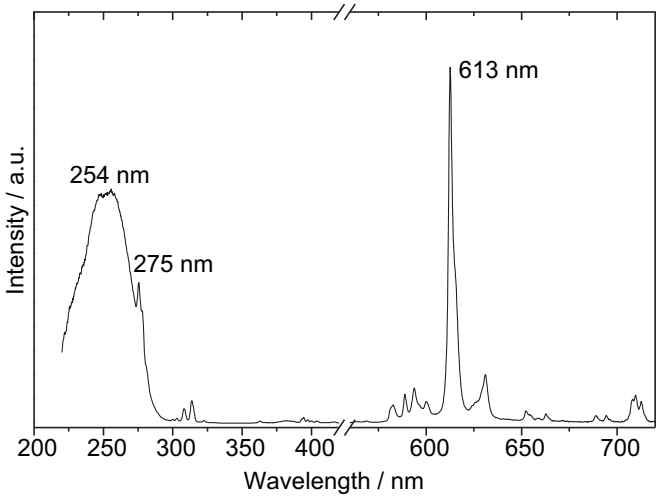

Fig. 5. Photoluminescence excitation and emission spectra of mesoporous Gd_2O_3:Eu (5 mol% doping).

3.4. Cell imaging and cytotoxicity

To check the possibility of the use of mesoporous Gd_2O_3:Eu nanoparticles as luminescent biological labels, we conducted *in vitro* biological experiments using human cervical carcinoma (HeLa) cells. A two-photon laser scanning confocal microscope operating at around a 380 nm excitation wavelength was applied to excite the Eu^{3+} dopants for luminescence. As a control experiment, HeLa cells alone show almost no background fluorescence upon excitation at 380 nm (not shown). Nonetheless, upon incubation, incorporation of mesoporous Gd_2O_3:Eu particles into HeLa cells was observed. Fig. 6 show bright-field optical and fluorescence microscopy images of HeLa cells after incubation with 0.2 mg/mL of Gd_2O_3:Eu particles for 24 h. As observed, the nanoparticles can permeate into the cell membrane and display bright intracellular luminescence from particles (Fig. 6b). These mesoporous nanoparticles clearly retained their intrinsic fluorescence upon cellular internalization. Moreover, the corresponding bright-field measurements taken after incubation with the nanoparticles confirmed that the cells were viable throughout the imaging experiments (Fig. 6a) and that there were no evident regions of cell death [24]. To check the spatial localization of foreign materials within the cells, we took a series of Z-stack images of the cell (e.g., top to bottom) at 1 μm "slice" intervals of the HeLa cells stained with Gd_2O_3:Eu particles. A representative fluorescence image (Fig. 6c) taken from an internal slice clearly shows a red fluorescence within the cells. This indicates that mesoporous Gd_2O_3:Eu nanoparticles are localized within the interior environment of the HeLa cells. Similarly, our previous work and those by other groups have observed the cellular internalization of lanthanide-based nanoparticles including oxides (e.g., Gd_2O_3:Eu/Tb) [16,19], phosphates (e.g., $CePO_4$:Tb, $TbPO_4$:Eu) [24,25], vanadiums (e.g., YVO_4:Eu) [23] and fluorides (e.g., Na(Y, Gd)F_4:Yb,Er) [20,26–28].

Non-toxicity is also an important feature for biological uses of nanoparticles. To check whether these mesoporous Gd_2O_3:Eu nanoparticles are biologically nontoxic and biocompatible, The particle-induced cytotoxic effects on HeLa cells were evaluated by conducting MTT (3-(4,5-dimethylthiazol-2-yl)-2,5-diphenyltetrazolium bromide) assays. The viability of untreated cells was assumed to be 100%. Fig. 7 shows the effect of Gd_2O_3:Eu nanoparticles on cell viability as a function of particle concentration and incubation time. The Gd_2O_3:Eu particles were almost not toxic to the cells even if a high concentration of 0.2 mg/mL particles were incubated with the HeLa cells for long time of 72 h. This indicates that the mesoporous Gd_2O_3:Eu particles alone possess a considerable biocompatibility. These results demonstrate high potential of lanthanide-based luminescent nanomaterials toward applications in bio-imaging and bio-labeling because of their internalization inside cells, observed intracellular luminescence, and rather low cytotoxicity.

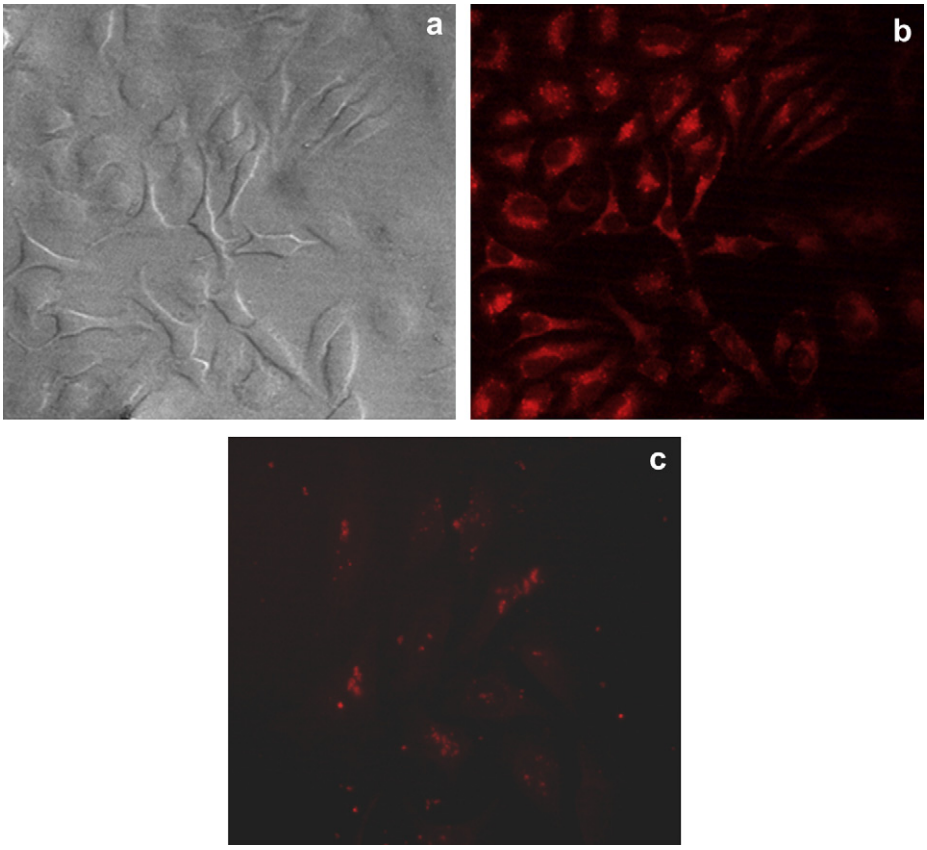

Fig. 6. Bright-field (a) and fluorescence microscopy (b) images of HeLa cells incubated with mesoporous Gd_2O_3:Eu nanoparticles, and a representative fluorescence image of HeLa cells stained with mesoporous Gd_2O_3:Eu nanoparticles from an internal slice (c).

3.5. *In vitro* drug storage and release

To study the drug storage and release behavior of our present single-phased mesoporous Gd_2O_3:Eu, doxorubicin hydrochloride (DOX), a typical and widely used anticancer was selected as a model drug to investigate the loading amount, encapsulation efficiency and *in vitro* interaction with cancer cells. The mesoporous Gd_2O_3:Eu was loaded with DOX by soaking them in a concentrated drug-PBS (phosphate-buffered saline, pH 7.4) solution. The drug-loaded particles were collected by centrifugation and washing three times followed by drying under vacuum. By using UV–vis absorption spectroscopy, the drug loading content can be evaluated by comparing the absorption of the supernatant and washed solutions with that of original DOX solution at a wavelength of 233 nm. Based on absorption measurements, approximately 31.5 μg of drug molecules were stored inside 1 mg of mesoporous Gd_2O_3:Eu particles. The loading efficiency

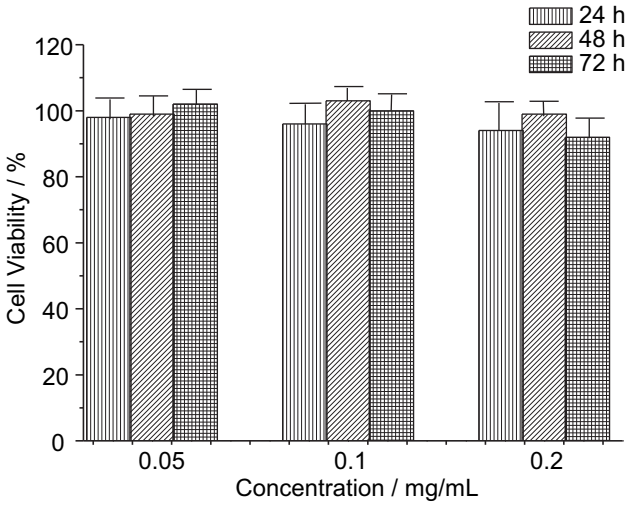

Fig. 7. The viability of HeLa cells incubated with mesoporous Gd_2O_3:Eu particles as a function of particles concentration and incubation time.

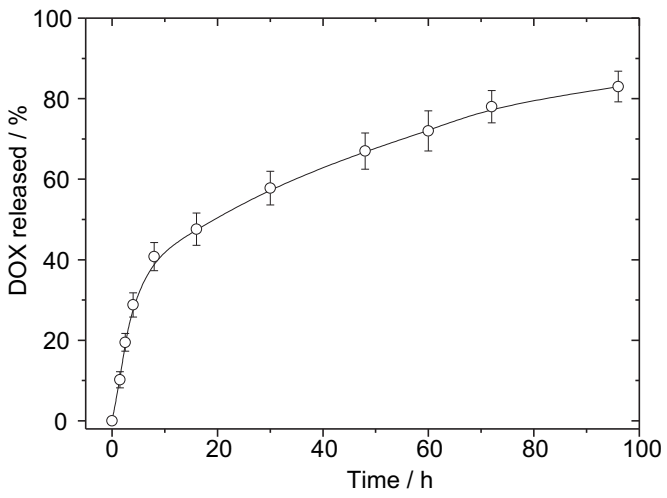

Fig. 8. Release profile of DOX from DOX-loaded mesoporous Gd_2O_3:Eu particles in PBS at 37 °C.

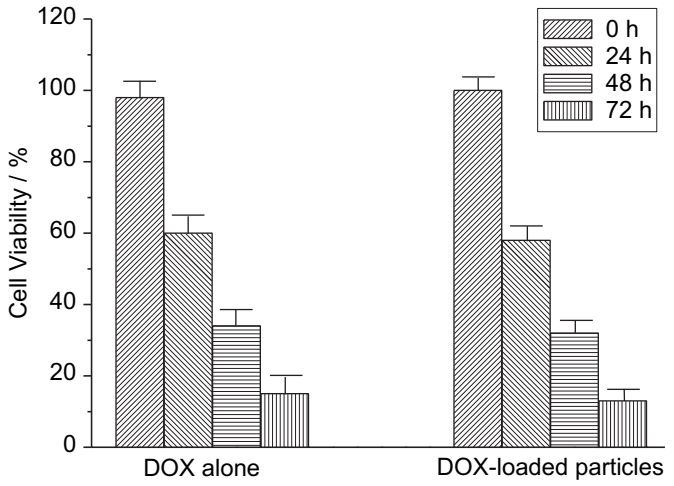

Fig. 9. The viabilities of HeLa cells inbubated with free DOX and DOX-loaded Gd_2O_3:Eu particles, respectively, as a function of time. The concentrations of DOX and particles are 15 μg/mL and 200 μg/mL, respectively.

of DOX was calculated as follows: $E\% = (O_{DOx}\text{-}R_{DOx})/O_{DOx} \times 100\%$, where O_{DOx} and R_{DOx} are the original and residual DOX content, respectively. The loading efficiency of DOX was 78.8%, indicating a relatively high loading efficiency of our present mesoporous lanthanide oxide.

To evaluate the release behavior of DOX-loaded Gd_2O_3:Eu particles, the particles were redispersed in PBS solution at 37 °C. Similarly, the drug release content was evaluated by using UV–vis absorption spectroscopy. Fig. 8 shows the release profile of the drug from DOX-loaded mesoporous Gd_2O_3:Eu particles. Approximately 40% of the drug was released from mesopores within 8 h followed by a relatively slow release during the subsequent 88 h, achieving the total release of 83% of DOX within 96 h. This indicates that our present mesoporous Gd_2O_3:Eu particles loaded with DOX obviously had a sustained drug release behavior, and such kinetics would be especially useful for effective treatment of cancer cells. These results demonstrate that single-phased mesoporous Gd_2O_3:Eu can be potentially used as an efficient vehicles to load and deliver anticancer drugs into cancer cells.

3.6. Pharmacological effect

To verify whether the released DOX was pharmacologically active, the cytotoxic effect of the DOX-loaded particles against HeLa cells was assessed by using MTT assays. Fig. 9 shows the cell viabilities against free DOX and DOX-loaded Gd_2O_3:Eu particles. The DOX-loaded Gd_2O_3:Eu particles induced a significant cytotoxicity that was demonstrated by the decreased cell viability upon incubation of DOX-loaded particles with HeLa cells. As revealed before, the Gd_2O_3:Eu particles alone are almost nontoxic. This means that the toxicity of the DOX-loaded Gd_2O_3:Eu particles originates from the release of drug molecules inside the cells. The trend of cell viability as a function of incubation time is consistent with that of drugs release. Moreover, the cytotoxic effect of DOX-loaded particles against the HeLa cells is comparable to the case for free DOX. This indicates that the loaded DOX keeps its pharmaceutical activities. Therefore, the porous Gd_2O_3 nanoparticles have capability to kill the cancer cells when loaded with the anticancer drugs, indicating the potential of treatment of tumors.

4. Conclusions

In summary, the concept of single-phased mesoporous lanthanide oxides as multifunctional biomaterials has been demonstrated by using Gd_2O_3:Eu as an example of a promising platform for simultaneous drug delivery and cell imaging. The spherical mesoporous Gd_2O_3 nanoparticles were prepared by a simple template-free solid-state-chemistry based thermal decomposition process of lanthanide complex sources. The porous features of obtained nanoparticles were demonstrated by TEM observation and nitrogen adsorption-desorption isotherm, showing well-defined mesopores, large pore size and volume, and high specific surface area. Biological experiments revealed that the single-phase mesoporous Gd_2O_3:Eu possesses the capability of the storage and release of drugs. Cytotoxicity assays demonstrated that the DOX-loaded mesoporous nanoparticles were able to induce cancer cells death efficiently through the sustained release of anticancer drugs within the cells, indicating the potential for treatment of tumors. Furthermore, the Gd_2O_3:Eu nanoparticles shows strong intracellular luminescence upon incubation with the HeLa cells, giving the function of cell imaging simultaneously. Therefore, single-phased luminescent mesoporous Gd_2O_3:Eu nanoparticles, that combine the capabilities of drug storage/release and simultaneous optical imaging, provide a potential platform for multifunctional biological uses. In comparison with those multicomponent composite/hybrid nanostructures, single-phased multifunctional nanoparticles have several advantages such as ease of preparation, homogeneity of morphology and properties, and stability and reproducibility of applications.

Acknowledgements

This study was partly supported by the Grant-in Aid for Scientific Research of the JSPS and the World Premier International Research (WPI) Center Initiative on Materials Nanoarchitronics (MANA), MEXT, Japan and the National High Technology Research and Development Program of China (863 program: 2009AA03Z309).

Appendix. Supplementary material

Supplementary data associated with this article can be found, in the online version, at doi: 10.1016/j.biomaterials.2011.06.019.

References

[1] Zhu Y, Ikoma T, Hanagata N, Kaskel S. Rattle-type Fe_3O_4@SiO_2 hollow mesoporous sphere as carriers for drug delivery. Small 2010;6:471–8.
[2] Chen Y, Chen H, Zeng D, Tian Y, Chen F, Feng J, et al. Core/shell structured hollow mesoporous nanocapsules: a potential platform for simultaneous cell imaging and anticancer drug delivery. ACS Nano 2010;4:6001–13.
[3] Torchilin Micellar Nanocarriers V. Pharmaceutical Perspectives. Pharm Res 2007;24:1–16.
[4] Kresge C, Leonowicz M, Rhth W, Vartuli J, Beck J. Ordered mesoporous molecular sieves synthesized by a liquid-crystal template mechanism. Nature 1992;359:710–2.
[5] Hartmann M. Ordered mesoporous materials for bioadsorption and biocatalysis. Chem Mater 2005;17:4577–93.
[6] Qian H, Guo H, Ho P, Mahendran R, Zhang Y. Mesoporous-silica-coated upconversion fluorescent nanoparticles for photodynamic therapy. Small 2009; 5:2285–90.
[7] Yang P, Quan Z, Hou Z, Li C, Kang X, Cheng Z, et al. A magnetic, luminescent and mesoporous core-shell structured composite material as drug carrier. Biomaterials 2009;30:4786–95.
[8] Liong M, Lu J, Kovochich M, Xia T, Ruehm S, Nel A, et al. Multifunctional inorganic nanoparticles for imaging, targeting, and drug delivery. Acs Nano 2008;5:889–96.
[9] Cho HS, Dong ZY, Pauletti GM, Zhang JM, Xu H, Gu HC, et al. Fluorescent, superparamagneticc nanospheres for drug storage, targeting, and imaging: a multifunctional nanocarrier system for cancer diagnosis and treatment. ACS Nano 2010;4:5398–404.
[10] Hifumi H, Yamaoka S, Tanmoto A, Citterio D, Suzuki K. Gadolinium-based hybrid nanoparticles as a positive MR contrast agent. J Am Chem Soc 2006; 128:15090–1.
[11] Foy S, Manthe R, Foy S, Dimitrijevic S, Krishnamurthy N, Labhasetwar V. Optical imaging and magnetic field targeting of magnetic nanoparticles in tumors. ACS Nano 2010;4:5217–24.

[12] Shi D, Cho H, Chen Y, Xu H, Gu H, Lian J, et al. Fluorescent polystyrene-Fe_3O_4 composite nanospheres for *in vivo* imaging and hyperthermia. Adv Mater 2009;21:2170–3.
[13] Zhelev Z, Ohba H, Bakalova R. Single quantum dot-micelles coated with silica shell as potentially non-cytotoxic fluorescent cell tracers. J Am Chem Soc 2006;128:6324–5.
[14] Zhang C, Li C, Peng C, Chai R, Huang S, Yang D, et al. Facile and controllable synthesis of monodisperse CaF_2 and CaF_2:Ce^{3+}/Tb^{3+} hollow spheres as efficient luminescent materials and smart drug carriers. Chem Eur J 2010;16:5672–80.
[15] Matijevic E, Hsu W. Preparation and properties of monodispersed colloidal particles of lanthanide compounds: I. gadolinium, europium, terbium, samarium, and cerium(III). J Colloid Interface Sci 1987;118:506–23.
[16] Lechevallier S, Lecante P, Mauricot R, Dexpert H, Dexpert-Ghys J, Kong HK, et al. Gadolinium-eupopium carbonate particles: controlled precipitation for luminescent biolabeling. Chem Mater 2010;22:6153–61.
[17] Yu C, Zhang L, Shi J, Zhao J, Gao J, Yan D. A simple template-free strategy to synthesize nanoporous manganese and nickel oxides with narrow pore size distribution and their electrochemical properties. Adv Funct Mater 2008;18: 1544–54.
[18] Xia GD, Wang SM, Zhou SM, Xu J. Selective phase synthesis of a high luminescence Gd_2O_3:Eu nanocrystal phosphor through direct solution combustion. Nanotechnology 2010;21:345601.
[19] Setua S, Menon D, Asok A, Nair S, Koyakutty M. Folate receptor targeted, rare-earth oxide nanocrystals for bi-modal fluorescence and magnetic imaging of cancer cells. Biomaterials 2010;31:714–29.
[20] Bai X, Song H, Pan G, Lei Y, Wang T, Ren X, et al. Size-dependent upconversion luminescence in Er^{3+}/Yb^{3+}-codoped nanocrystalline yttria: Saturation and thermal effects. J Phys Chem C 2007;111:13611–7.
[21] Lu S, Zhang J, Zhang J, Zhao H, Luo Y, Ren X. Remarkably enhanced photoluminescence of hexagonal $GdPO_4nH_2O$: Eu with decreasing size. Nanotechnology 2010;21:365709.
[22] Di W, Wang X, Chen B, Lu S, Zhao X. Effect of OH^- on the luminescent efficiency and lifetime of Tb^{3+} doped yttrium orthophosphate synthesized by solution precipitation. J Phys Chem B 2005;109: 13154–8.
[23] Shen J, Sun L, Zhu J, Wei L, Sun H, Yan C. Biocompatible bright YVO_4:Eu nanoparticles as versatile optical bioprobes. Adv Funct Mater 2010;20: 3708–14.
[24] Zhang F, Wong S. Ambient large-scale template mediated synthesis of high-aspect ratio single-crystalline, chemically doped rare-earth phosphate nanowires for bioimaging. ACS Nano 2010;4:99–112.
[25] Di W, Li J, Shirahata N, Sakka Y, Willinger M, Pinna N. Photoluminescence, cytotoxicity and *in vitro* imaging of hexagonal terbium phosphate nanoparticles doped with europium. Nanoscale 2011;3:1263–9.
[26] Zhou J, Sun Y, Du X, Xiong L, Hu H, Li F. Dual-modality in vivo Imaging using rare-earth nanocrystals with near-infrared to near-infrared (NIR-to-NIR) upconversion luminescence and magnetic resonance properties. Biomaterials 2010;31:3287–95.
[27] Jiang S, Zhang Y, Lim K, Sim E, Ye L. NIR-to-visible upconversion nanoparticles for fluorescent labeling and targeted delivery of siRNA. Nanotechnology 2009; 20:155101.
[28] Mi C, Zhang J, Gao H, Wu X, Wang M, Wu Y, et al. Multifunctional nanocomposites of superparamagnetic (Fe_3O_4) and NIR-responsive rare earth-doped up-conversion fluorescent ($NaYF_4$: Yb, Er) nanoparticles and their applications in biolabeling and fluorescent imaging of cancer cells. Nanoscale 2010;2:1141–8.